

RESEARCH ARTICLE | MARCH 26 2024

Numerical investigation of laser doping parameters for semi-insulating 4H-SiC substrate **FREE**

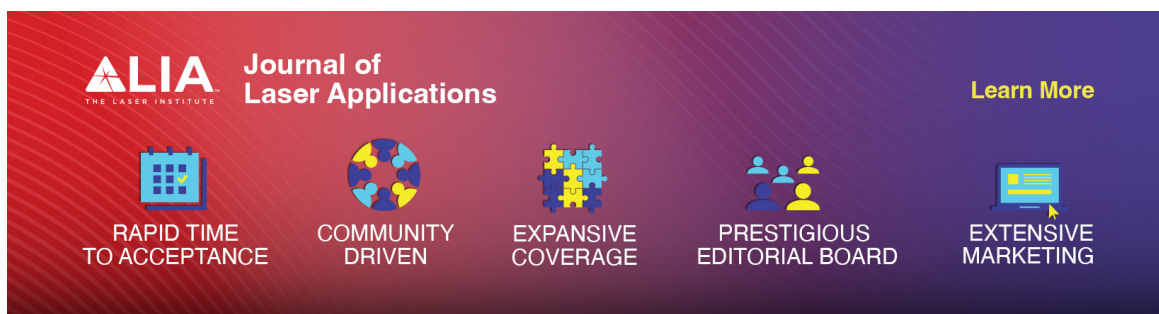
Special Collection: [Proceedings of the International Congress of Applications of Lasers & Electro-Optics \(ICALEO 2023\)](#)

Chandraika (John) Sugrim ; Gunjan Kulkarni ; Yahya Bougdid ; Kevin Heylman ; Ranganathan Kumar ; Aravinda Kar  ; Kalpathy Sundaram 

 Check for updates

J. Laser Appl. 36, 022013 (2024)






<https://doi.org/10.2351/7.0001158>



ALIA
THE LASER INSTITUTE

Journal of Laser Applications

[Learn More](#)

-  **RAPID TIME TO ACCEPTANCE**
-  **COMMUNITY DRIVEN**
-  **EXPANSIVE COVERAGE**
-  **PRESTIGIOUS EDITORIAL BOARD**
-  **EXTENSIVE MARKETING**

ALIA
THE LASER INSTITUTE

Numerical investigation of laser doping parameters for semi-insulating 4H-SiC substrate

Cite as: J. Laser Appl. 36, 022013 (2024); doi: 10.2351/7.0001158

Submitted: 3 July 2023 · Accepted: 29 February 2024 ·

Published Online: 26 March 2024



Chandraika (John) Sugrim,^{1,2} Gunjan Kulkarni,^{1,2} Yahya Bougdid,^{2,3} Kevin Heylman,⁴
Ranganathan Kumar,³ Aravinda Kar,^{1,2,a)} and Kalpathy Sundaram¹

AFFILIATIONS

¹Department of Electrical and Computer Engineering, University of Central Florida, Orlando, Florida 32816

²Center for Research and Education in Optics and Photonics (CREOL), The College of Optics and Photonics, University of Central Florida, Orlando, Florida 32816

³Department of Mechanical and Aerospace Engineering, University of Central Florida, Orlando, Florida 32816

⁴EOSPACE Inc., 6222 185th Ave NE, Suite 100, Redmond, Washington, DC 98052

Note: Paper published as part of the special topic on Proceedings of the International Congress of Applications of Lasers & Electro-Optics 2023.

^{a)}Author to whom correspondence should be addressed; electronic mail: akar@creol.ucf.edu

ABSTRACT

Semi-insulating (SI) 4H-polytype of silicon carbide (SiC) is a highly desirable wide bandgap semiconductor material for various applications in challenging environments owing to its exceptional characteristics such as high melting point, remarkable thermal conductivity, strong breakdown field, and excellent resistance to oxidation. This study investigates the critical laser processing parameters to operate a pulsed UV 355 nm laser to dope high-purity (HP) SI 4H-SiC substrates with boron. The doping process parameters are examined and simulated for this UV laser doping system using a liquid precursor of boron. Boron atoms create a dopant energy level of 0.3 eV in the doped HP 4H-SiC substrates. Diffusion of boron atoms into 4H-SiC substrates modifies the hole density at 0.3 eV energy level, and causing a variation in the dynamic refraction index, and absorption index. Consequently, the optical properties of boron doped samples, namely, transmittance, reflectance, and absorbance, can be modified. The current simulation reported in this study explains the motivation of UV optical doping strategy to dope SiC substrates. A beam homogenizer was used to control the laser spot used to generate doping process. The advantage of the beam homogenizer is demonstrated by producing flat-top beams with uniform intensity over a certain area defined by the focusing lens choice. A simple theoretical model is used to select the laser processing parameters for doping SiC substrates. These modeled parameters are used to determine the efficient laser processing parameters for our doping experiments.

Key words: laser doping, 4H-SiC substrate, boron, beam homogenizer, Gaussian beam, flat-top beam, refraction index

Published under an exclusive license by Laser Institute of America. <https://doi.org/10.2351/7.0001158>

I. INTRODUCTION

Semi-insulating 4H-polytype of silicon carbide (SiC) is a highly desirable indirect wide bandgap semiconductor material for advanced electro-optical devices.¹ The covalent bonds between silicon (Si) and carbon (C) atoms enable SiC substrates to have a large bandgap energy of ~ 3.2 eV.² Because of their hexagonal crystal structure, SiC semiconductors promote outstanding optical and thermal properties in addition to other exceptional physical characteristics such as a high melting point, thermal conductivity,

and electrical conductivity.³ The 4H- and 6H-polytypes of SiC are uniaxial, making it an excellent material to control the optical refraction index.⁴ Compared to their silicon material counterparts, SiC substrates have many advantages for laser doping technology for fabricating micro- and optoelectronics devices; for example, 4H-SiC has a very large breakdown field of 2.8 MV/cm, that is about ten times larger than that of Si material.⁵ The losses in electronic devices fabricated by laser doping of SiC semiconductors are several hundred times lower than that of Si-based devices.⁵ SiC

29 March 2024 15:15:17

exists under several polymorphic types, and the most common phases available in industry and research are the hexagonal (4H-SiC and 6H-SiC) and cubic (3C-SiC) polycrystalline structures.²⁻⁴ The laser-doped 4H-SiC or 6H-SiC can be used in different applications, such as the resonant tunable waveguides, microactuators, microsensors, optical detectors, and integrated circuits (IC) in functional microelectronics devices, as reported in Refs. 6-8. Laser doping technique has been employed in semiconductor technology to assist the diffusion of dopant atoms into different n-type and p-type SiC substrates. The precursor atoms used in laser doping technology can be gallium (Ga), aluminum (Al), boron (B), chromium (Cr), and neodymium (Nd).⁹ However, because of the solid-state diffusion of dopant atoms (e.g., Ga or Al), laser doping of SiC should be realized only at a higher temperature; for example, around ~ 2100 K as reported by Salama *et al.*¹⁰ Many other techniques can be used for creating p-n-junction SiC devices, for example, ion implantation followed by subsequent annealing treatment at high temperatures above 1500°C , and the high-temperature implantation strategy can also be applied to prepare high-quality aluminum doped p-type layer in n-type silicon carbide semiconductors.^{11,12} However, the above-mentioned methods can create many defects in the fabricated SiC devices during the processing at high temperature. To overcome these challenges, optical laser doping techniques can provide high-quality doped SiC junction devices at ambient temperature using different laser wavelengths, e.g., 355, 532, or 1064 nm, for fabricating high-temperature and high-power electronic devices for different applications.³⁻⁵

Fuyuki *et al.*¹³ investigated shallow laser doping in crystalline Si solar cell fabrication using a 355 nm laser. The diffusion depths of dopants, i.e., phosphorus and boron atoms, were accurately controlled at the substrate surface to be under a depth of 0.3 mm by optimizing the doping processing parameters, as reported in Ref. 13. Pulsed 355 nm laser doping of p-type monocrystalline Si substrates using both phosphorus and boron precursors for the fabrication of silicon solar cells was experimentally demonstrated.¹³ Compared to high-cost and complex laser nanofabrication

techniques, for example, two-photon nanolithography,^{14,15} and ion implantation followed by thermal annealing,¹¹ pulsed laser doping method presents many advantages, and it can be performed at ambient temperature in air with micrometric laser-SiC interaction, resulting in a selective doping process for different applications.^{1,3,4} Lim and Kar⁴ used laser doping technique to dope n-type 4H-SiC substrates with Ga for developing an uncooled midwave infrared (MWIR) detector. Fourier-transform infrared spectroscopy (FTIR) measurements of the doped SiC sample demonstrated the creation of an acceptor energy of 0.30 eV which is caused by the incorporation of Ga dopant atoms into the SiC semiconductor.⁴ The Ga dopant modifies the electron density in the doped 4H-SiC, resulting in a change in the optical refraction index and absorption index.^{4,5}

In the current study, we developed a novel experimental model for an 355 nm laser doping system to dope SI HP 4H-SiC with boron atoms in order to fabricate MWIR resonant waveguides. A simple heat transfer thermal model is also used to select and predict the laser processing parameters, corresponding to the doping temperature, in order to incorporate the boron dopant atoms into SiC substrates without melting or damaging the SiC substrates. The laser doping experiments based on our simulation will be carried out using the processing parameters corresponding to temperatures below the peritectic temperature of 4H-SiC (i.e., 2830°C) according to Refs. 4 and 5. As reported by Feng *et al.*,¹⁶ SI HP 4H-SiC does not have a high concentration of impurities, thereby reducing the shift of the trap energy state from the center of the 3.2 eV bandgap. The SI HP 4H-SiC is chosen for our study as the recording medium semiconductor based on the above-mentioned reasons. Without a compensating deep level of vanadium (V) in the SiC, free charges have greater mobility. Additionally, not having vanadium dopant in SiC semiconductors reduces the number of scattering sites for a functional optical waveguide.¹⁷ FTIR spectrometry measurements, i.e., transmittance, reflectance, and absorptance, of the SI HP 4H-SiC samples were carried out to select the proper laser wavelength corresponding to the high absorptance and also to select the laser processing parameters for our doping experiments using a simple heat transfer model.

29 March 2024 15:15:17

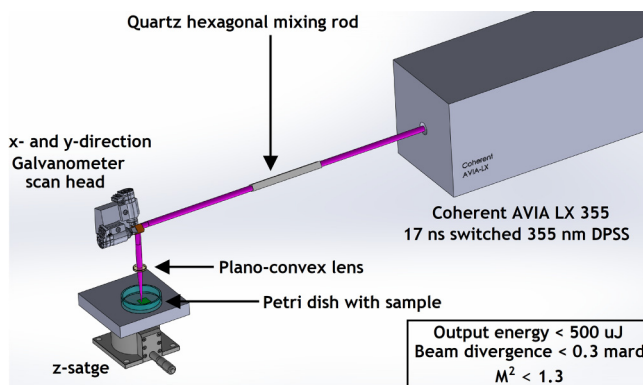


FIG. 1. Schematic illustration of the optical setup used in this study for laser doping of semi-insulating HP 4H-SiC semiconductor.

II. DESIGN OF EXPERIMENT, SIMULATION, AND SELECTION OF LASER PROCESSING PARAMETERS

A. Laser doping setup: Experimental and simulation

The experimental setup of our work is designed with three main goals in mind: (i) the ease of use in getting samples in and out of the directed energy doping platform, (ii) the uniform power distribution of the laser source, and (iii) the simple modification in changing the laser spot size with respect to the z-position of the focal point of the focusing lens. Using an off-the-shelf mounted focusing lens, pulsed laser source ($\lambda = 355$ nm), quartz hexagonal mixing rod, linear z-translating stage, and a 2D galvanometer, the experimental design for our laser doping setup is being constructed as shown by the schematic illustration in Fig. 1.

From coherent, a 355 nm nanosecond (ns) Q-switched (AVIA LX 355-20) DPSS laser with an output energy of about $500\mu\text{J}$ and a 25 ns pulse width is used as a light source for our doping

experiments. The laser's beam diameter of 3 mm size is then processed by a mixing rod and a lens combination to induce diffusion of dopant atoms into the SiC substrates. The divergence of laser radiation is 0.3 mrad (full angle) with a M^2 less than 1.3, where M^2 is the measured degree of variation of a beam from the ideal Gaussian beam.

In order to generate a uniform heating intensity profile of the laser beam on the SiC substrate surface, the Gaussian beam coming from the laser source is shaped into a uniform flat-top intensity profile by incorporating a quartz hexagonal mixing rod in the optical setup to integrate the original Gaussian laser beam, as presented in the schematic illustration of our setup in Fig. 1.

The propagation of the laser beam through the quartz hexagonal mixing rod shown in Fig. 2 is examined in Zemax's

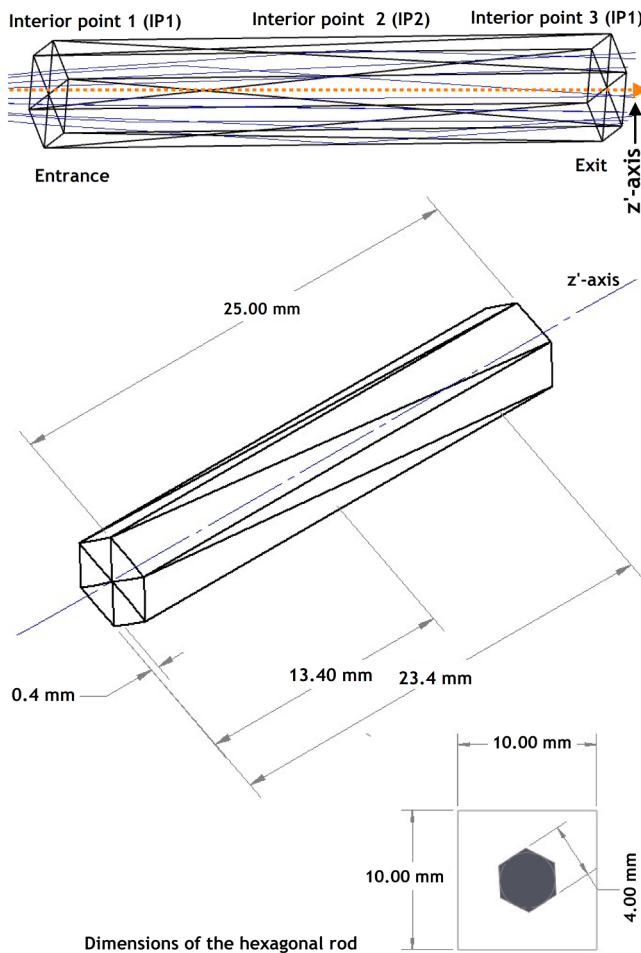


FIG. 2. The ray traces of a coherent Gaussian beam passing through the quartz hexagonal mixing rod with three sampling detectors which are positioned at mid-section location, at the input location, and at exit location. The length of the hexagonal rod is 25 mm, the width of the rod is 4 mm, and the length of one side of the hexagon is 2.31 mm. The front surface of the hexagonal mixing rod is placed in the x-y sampling plane.

OpticStudio using a coherent Gaussian laser source to illustrate the laser source radiation which is normal to the mixing rod. The laser irradiance is examined at five x- and y-plane perpendicular to the z'-axis (propagation axis) [i.e., (i) at the entrance before the mixing rod, (ii) 0.4 mm into the mixing rod interior point 1 (IP1), (iii) 13.4 mm into the mixing rod interior point 2 (IP2), (iv) 23.4 mm into the mixing rod interior point 3 (IP3), and at 1 mm after the mixing rod] of the quartz hexagonal mixing rod to determine the x-y surface plane irradiance profile during its propagation through the mixing rod, as presented in Fig. 2. The dimensions of each sampling plane are $10 \times 10 \text{ mm}^2$ which is 2.5 times the area of the hexagonal x-y surface plane.

The flatness of the 355 nm laser irradiance profile at the output of the exit pupil of the hexagonal mixing rod depends on the number of bounces that occur within the mixing rod. The total internal reflection of the quartz device causes mixing points in the laser beam as the beam propagates through the hexagonal quartz mixing rod device, as demonstrated in Fig. 2. All the dimensions of the hexagonal rod are mentioned in Fig. 2.

In the simulation of the mixing rod irradiance shown in Figs. 3(a)–3(j), five $10 \times 10 \text{ mm}^2$ square detectors were placed to sample the irradiance before the mixing rod, three locations in the mixing rod, and after the mixing rod. The surface plane irradiance before the mixing rod presented in Fig. 3(a) is a Gaussian beam of diameter 3 mm. Figure 3(b) is the x-profile of the beam irradiance shown in Fig. 3(a). In OpticStudio, discrete rays are used; therefore, the output irradiance plots of the surface sampling detector reflect that granularity of the detector and the launched ray bundle. Surface irradiance localized at IP1 [Fig. 3(c)] is 0.4 mm from the entrance pupil. It can be seen from Fig. 3(c) that the Gaussian beam is broken up into spatial modes. The peak irradiance for each spatial mode is depicted in Fig. 3(d). Similarly, Figs. 3(e) and 3(g) show the spatial mode in the mixing rod. Likewise, Figs. 3(e) and 3(h) show the peak irradiance of the spatial modes. At 1 mm from the exit of the mixing rod, as shown in Fig. 3(i), the spatial profile transformed to a Gaussian shape. Figure 3(j) is the x-profile of the beam irradiance shown in Fig. 3(i).

With the paraxial ray tracing done in Zemax's OpticStudio, we continued our simulation analysis in MATLAB software using an idealized coherent Gaussian beam with a beam waist of $2w_0 = 3 \text{ mm}$ as the starting laser radiance profile. Figure 4(a) shows that the irradiance distribution of the laser beam is localized and focused on the central circle indicated by the yellow intense color in which the laser intensity reached its maximum.

A cross-sectional beam profile is illustrated in Fig. 4(b) showing the peak radiant flux of the pulsed laser beam in the x-plane. The laser intensity of the Gaussian beam is highest, and the peak radiant flux is localized at the center, and it exponentially decreases as it moves away from the center [Fig. 4(b)].

As presented in Fig. 5(a), our simulation demonstrated that the laser irradiance after the mixing rod and a 30 mm plano-convex lens the profile of the Gaussian beam diameter of 3 mm size is uniform in both x- and y-directions, thereby producing a flat-top beam. The peak irradiance profile of the 3 mm flat-top beam at the exit aperture of the plano-convex lens showed that the intensity distribution of the focused laser reached its maximum, i.e., the

29 March 2024 15:15:17

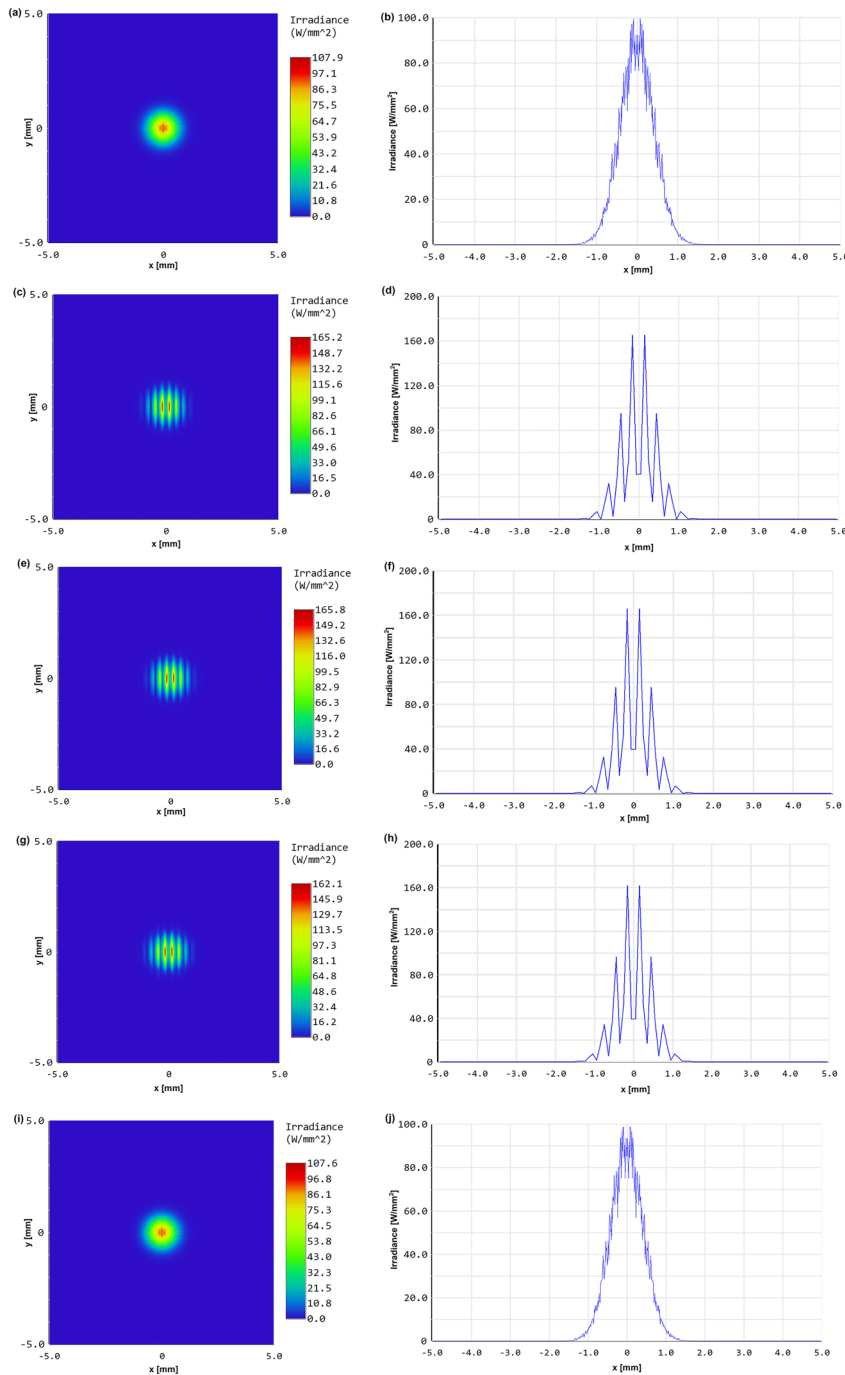


FIG. 3. (a) Laser irradiance at the x–y plane ($10 \times 10 \text{ mm}^2$) before the entrance pupil of the mixing rod. (b) 1D x-profile of the laser irradiance in (a). (c) Irradiance at the x–y plane at interior point 1 (IP1), i.e., at 0.4 mm from the entrance pupil. (d) 1D x-profile of the irradiance in (c). (e) Irradiance at the x–y plane at interior point 2 (IP2), i.e., at 13.4 mm from the entrance pupil. (f) 1D x-profile of the irradiance in (e). (g) Irradiance at the x–y plane at interior point 3 (IP3), i.e., at 23.4 mm from the entrance pupil. (h) 1D x-profile of the irradiance in (g). (i) Irradiance at the x–y plane at 1 mm from the exit of mixing rod. (j) 1D x-profile of the irradiance in (i).

29 March 2024 15:15:17

sharpness of the energy density transition. Shown in Fig. 5(b) is a 1D profile of the Gaussian laser beam in the x-plane.

Figures 5(a) and 5(b) show that the energy of the Gaussian beam reaches almost $\sim 100\%$ of its maximum and it localized in the minimum area of the laser focus center, thus confirming the success of simulation discussed in this study.

In our study, we further investigated the behavior of the intensity distribution when the laser spot is positioned in and out of focus as a function of the focal distance of the lens from the working surface. By changing the depth of the focus, i.e., controlling the z-position of the focal spot, different profiles of the laser irradiance distribution on the sample are investigated. It was

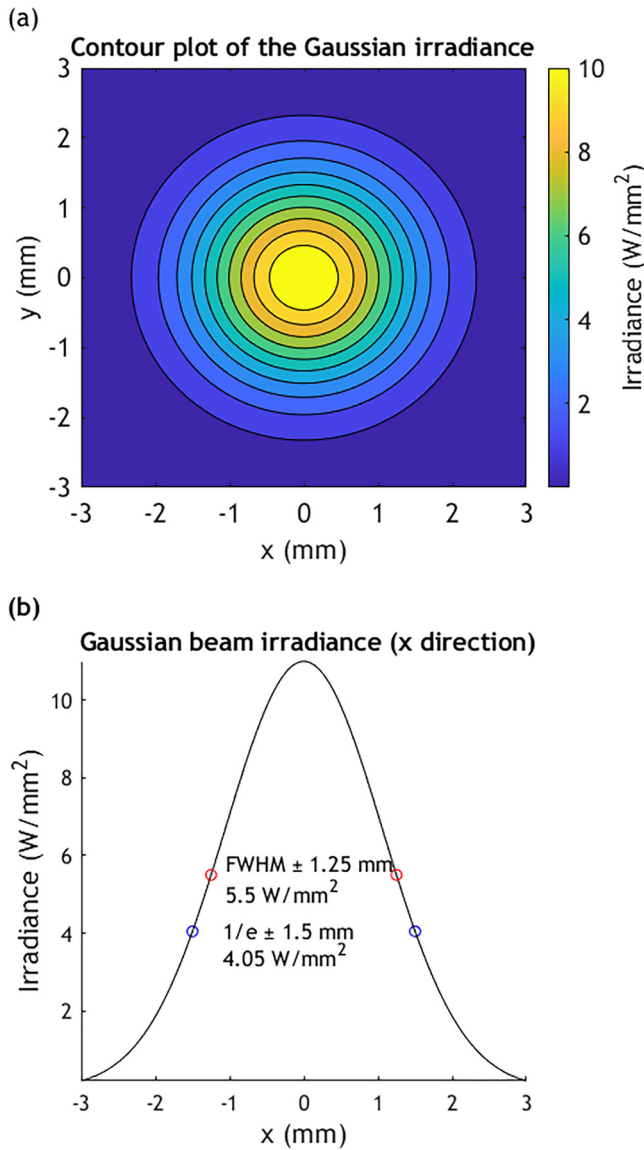


FIG. 4. (a) Irradiance of an idealized Gaussian laser profile with a beam waist of $2W_0 = 3$ mm. (b) 1D profile of the irradiance distribution of the Gaussian laser beam in the x-direction.

previously reported¹⁴ that the size of the interaction area of the laser spot with the irradiated material can be changed as a function of the z-position of the focal point.

Shown in Figs. 6–8, 10, and 11 are the peak irradiance profiles and it is corresponding 1D x-profile of the 3 mm Gaussian beam at the exit aperture of the quartz hexagonal mixing rod and the 30 mm plano-convex lens at different focal distance of the laser spot from the working surface of the SiC substrate surface, i.e., the laser-SiC interaction zone where the doping triggered by the laser diffusion mechanism.^{1,4,5}

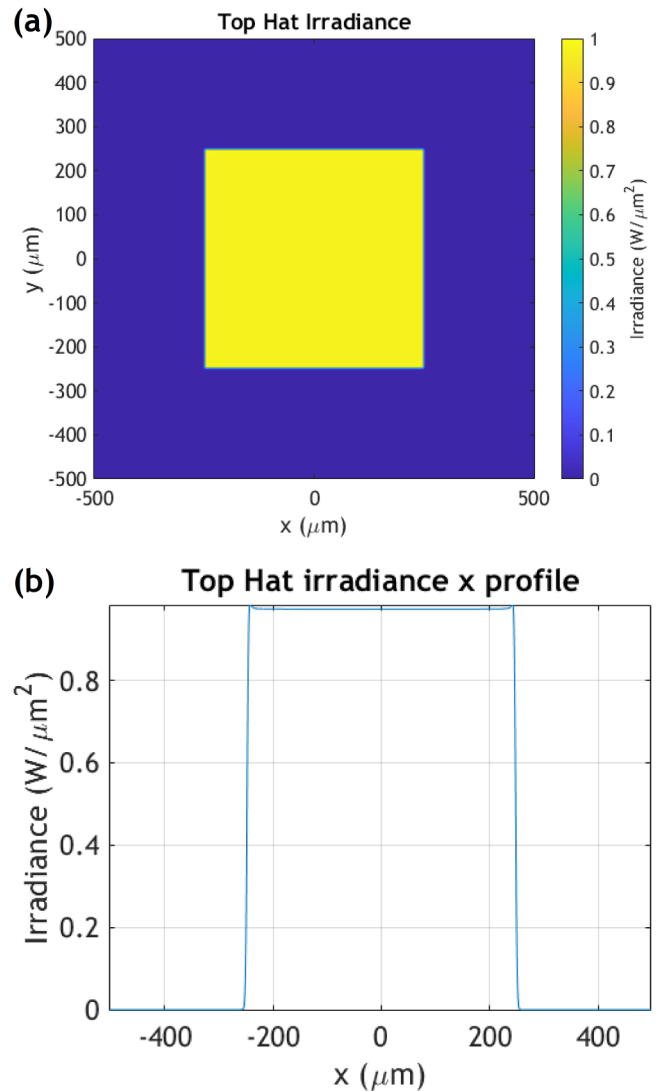


FIG. 5. (a) Peak irradiance of the 3 mm flat-top laser beam at the exit aperture of the hexagonal mixing rod and a 30 mm focal length lens at the focus. (b) Peak irradiance of the 3 mm flat-top beam in the x-plane after passing through the beam homogenizer and a 30 mm focal length lens at the focus.

According to the simulations shown in Figs. 6(a) and 6(b), we demonstrated that the proper focusing of the laser spot is important for getting a uniform and homogenous distribution of the laser-peak irradiance on the SiC surface in order to achieve maximum intensity and reach a threshold of temperature below the peritectic temperature of SiC to dope the SiC substrates with boron.

The simulation in Figs. 7(a) and 7(b) shows that a focal distance of -0.5 mm away from the focal point leads to a sharp roll-off of the irradiance and the laser-peak irradiance density area begins to contract in size. The focused laser spot in Figs. 8(a) and 8(b) shows a uniform and homogenous laser intensity distribution of

29 March 2024 15:15:17

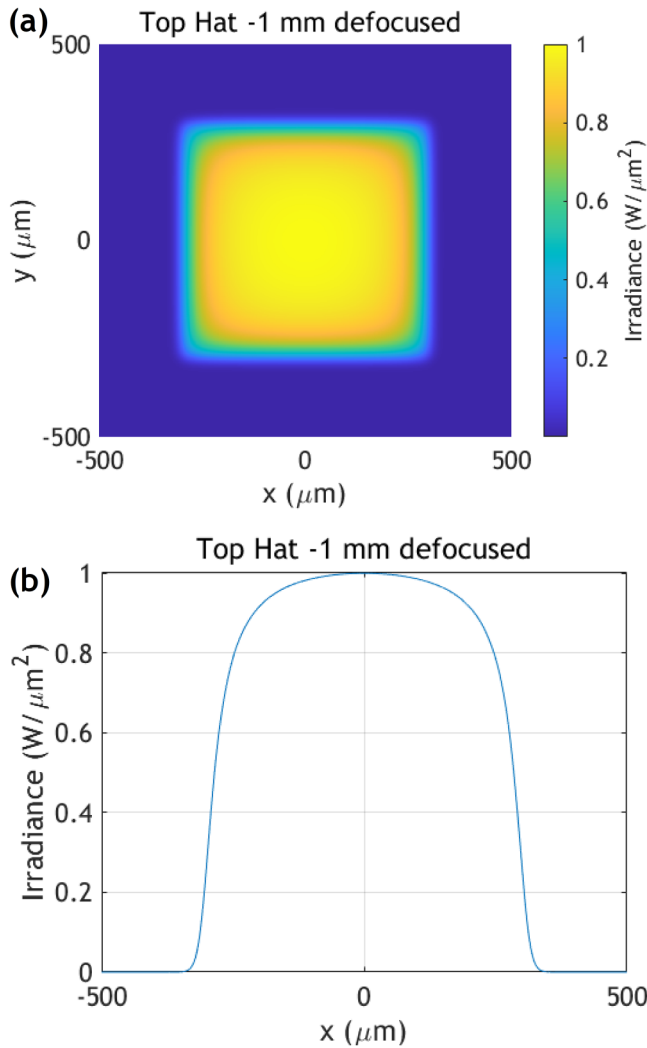


FIG. 6. (a) Peak laser irradiance profile and (b) peak irradiance x-profile of the 3 mm flat-top beam at the exit aperture of the mixing rod and the 30 mm plano-convex lens with -1 mm defocusing from the working surface at sample point SP1 (see Fig. 9).

the flat-top beam. The result in Fig. 8(a) was previously confirmed in Figs. 5(a) and 5(b).

In this simulation, a lens of short focal length, i.e., 30 mm, is used to obtain a very small focal spot of $2w_0 = 0.6 \mu\text{m}$. The peak laser irradiance should be approximately the same within the $2z_R$ (twice of the Rayleigh length) region.¹⁴ After the Rayleigh range, the beam diverges rapidly resulting in significant variation in the peak irradiance profile because the Fresnel diffraction dominates the irradiance distribution.^{14,18}

The irradiance profiles change as the beam propagates, which is due to the diffraction effect resulting in the spreading of the beam and the redistribution of the laser-peak irradiance.^{19,20} The

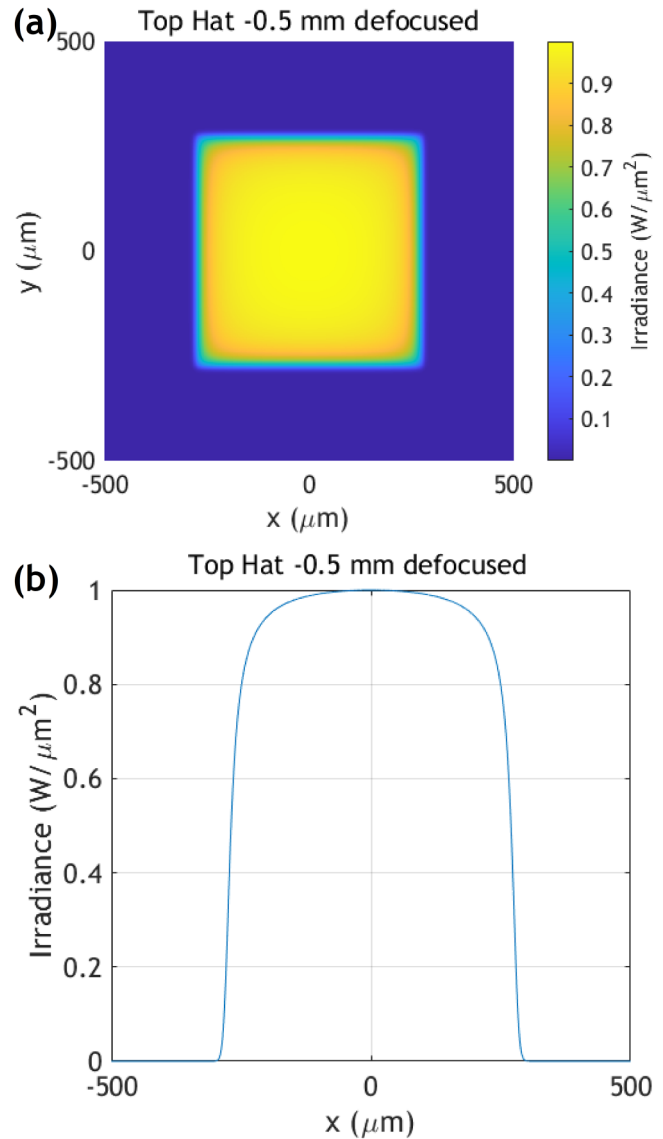


FIG. 7. (a) Peak laser irradiance profile and (b) peak irradiance x-profile of the 3 mm flat-top beam at the exit aperture of the mixing rod and the 30 mm plano-convex lens with -0.5 mm working surface defocusing at sample point SP2 (see Fig. 9).

variation in the total power at different planes may be due to the diffraction effects.

Within the Rayleigh range and the radiation envelope given by the hyperbolic function, the wavefronts are curved, and, therefore, these wavefronts have a positive curvature on the left of the beam waist (see Fig. 9). After the minimum position, which is the beam waist (focus), the wavefronts have a negative curvature. The Fresnel diffraction dominates in this region of collimated space. The power distribution changes because the Fresnel diffraction scatters the

29 March 2024 15:15:17

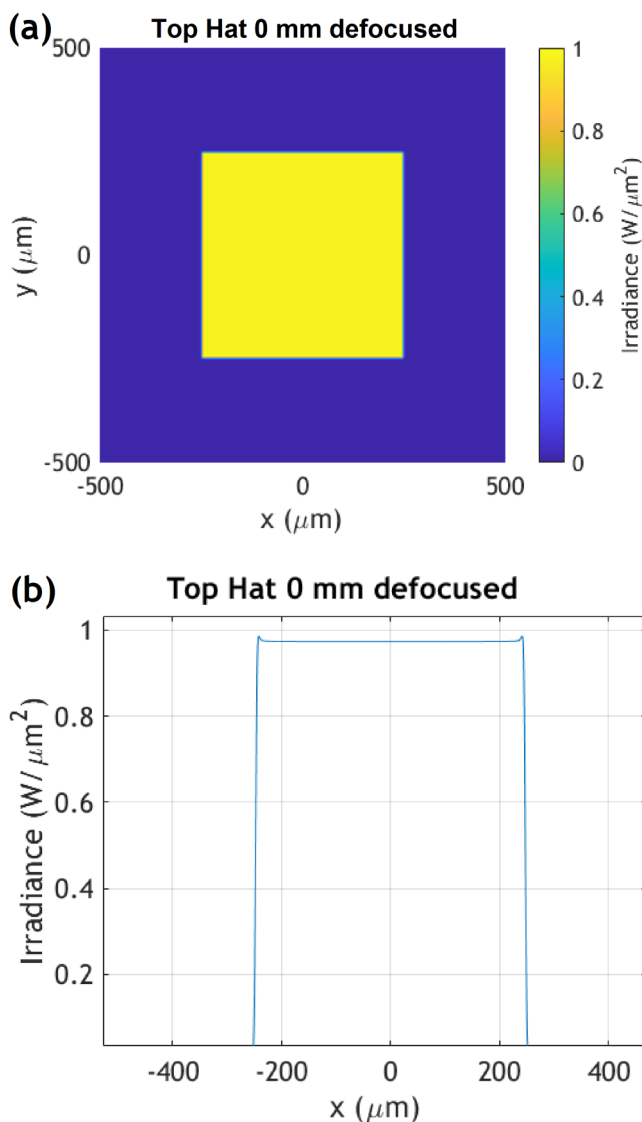


FIG. 8. (a) Peak laser irradiance and (b) x-profile of the peak irradiance at the focus ($z=0\ \mu\text{m}$). A homogeneous and intense laser irradiance is localized at the focus at sample point SP3 (see Fig. 9).

peak irradiance, resulting in a decrease in the spatial variation of the power. At the defocus position, the total irradiance is the same but the peak irradiance is different as Fresnel's diffraction starts to dominate. The decrease in peak irradiance due to Fresnel diffraction was previously reported in Refs. 19 and 20.

Figures 10(a), 10(b), 11(a), and 11(b) show how rapidly the laser-peak irradiance deteriorates. To obtain the optimal heating profile of the laser spot, a linear z-stage was added to the setup to control the z-position of the laser focus and, therefore, adjust the laser intensity distribution on the SiC surface. In order to dope the

SiC semiconductors using our home-made optical setup, the laser beam should scan the area of the surface of the SiC substrate that needs to be doped with an efficient laser intensity which will generate the temperature required to diffuse the dopant atoms into the substrate. To accomplish this, we coupled a two-axis galvanometer with our laser doping setup, as shown in Fig. 1. Technically, one arm of the galvanometer scanner is used to control the linear motion of the laser beam in the x-direction, and the other is used to control the motion in the y-direction. Our 2D motion of the stage is controlled by a home-made software, we have developed for our optical setup using micro-Hertz sine waves.

One of the principal benefits of the galvanometer scanner system is that it adds a correction factor for the breaking of the telecentric system introduced by the hexagonal mixing rod. The galvanometer can reorient the laser beam perpendicular to the SiC substrate that needs to be doped. The other advantage of the galvanometer scanner system which provides is a means for us to add dampeners to the substrate holder to lessen the impact of mechanical shock caused by the laser energy hitting the surface of the SiC substrate. The third advantage of the scanning system given by the galvanometer scanner is the freedom to work with fairly large area (Fig. 1).

The x-position of the laser beam on the SiC substrate surface is determined by the perpendicular height d of the center of the galvanometer x-axis's mirror multiplied by the sine of the angle (θ_x) that the galvo's mirror makes with respect to the SiC substrate surface, and similarly, the y-position is determined by the same geometrical relationship. In our experiment, the interaction time between the laser and the SiC substrate during the doping process can be determined by the following equation:

$$\tau_{int} = \frac{L_{spot\ size}}{\omega} \quad (1)$$

where $L_{spot\ size}$ is the laser spot size, which is focused on the SiC substrate surface, d is height of the center of galvanometer x-axis's mirror, and ω is the angular speed of the galvanometer scanner.

B. Determination of the scan rate, laser wavelength, and laser processing parameters for doping of SI 4H-SiC

Using a Perkin Elmer Lambda 365+ UV-Visible-NIR spectrometer, the optical properties, i.e., transmittance, reflectance, and absorptance of the SiC substrate were measured in order to use their data for selecting the laser wavelength and proper processing parameters (using the theoretical model) for doping SiC substrates. The optical properties of the HP SI 4H-SiC substrate used in this work were measured from 200 to 1100 nm, as shown in Fig. 12. From the absorptance data in Fig. 12, we determined the peak absorptance radiation at which the SiC substrate can absorb sufficient light required to trigger the thermal diffusion of boron, and, therefore, dope the SiC substrates. A pulsed UV laser emitted at 355 nm wavelength was found to be an ideal laser source of heating for our doping experiments. A reflectance of around 25% is detected at 355 nm for the undoped SiC substrate (Fig. 12). In the visible range of wavelength, i.e., from 400 to 700 nm, the HP SI 4H-SiC substrate is highly transparent (Fig. 12).

29 March 2024 15:15:17

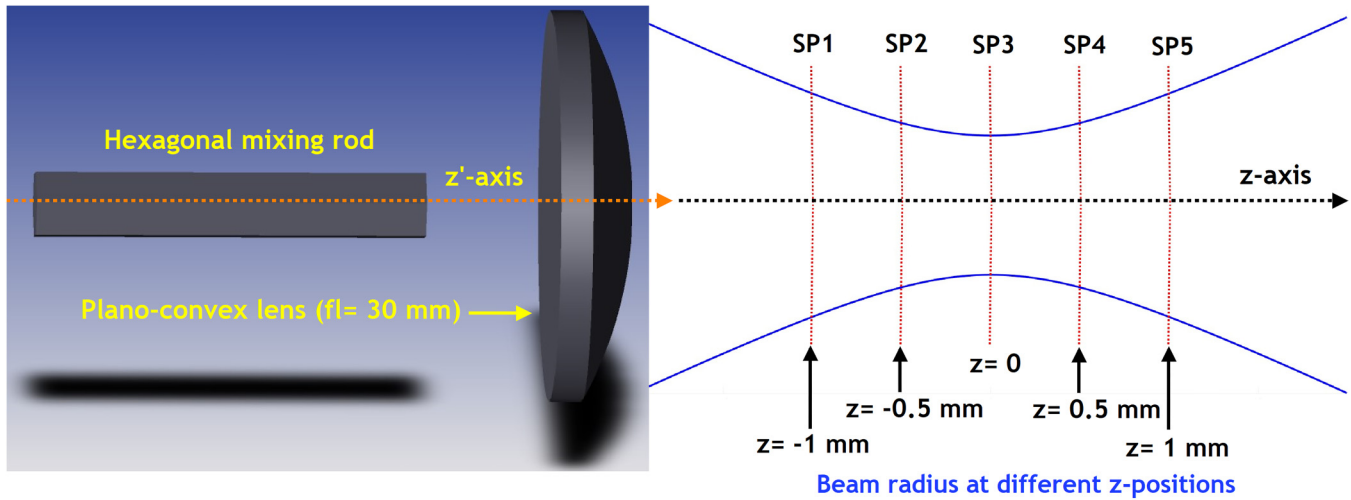


FIG. 9. Flat-top laser beam as a function of the z -position with respect to the beam w_0 . $2 w_0$ denotes the minimum beam diameter at the focus. The red dotted line indicates where the peak irradiance are sampled starting from the left of the plot. Sample point 1 (SP1) to SP5 are used to demonstrate how quickly the irradiance drops outside of z_R .

By choosing 355 nm laser line according to Fig. 12, a Coherent AVIA LX 355 laser was selected as the heating source for doping SiC. According to the simulation investigation in this paper, the 355 nm laser can be efficiently used to dope the SI HP 4H-SiC substrate, as previously reported by Boutopoulos *et al.*²¹ With a 355 nm laser and an initial laser spot size of 3 mm selected for the doping experiment, we developed a simple heat transfer theoretical model to determine the proper laser processing parameters necessary to select the proper temperature required to dope the SI HP 4H-SiC samples with boron. This simple heat transfer model was detailed in our previous published work.²² Equation (2) is used to calculate the temperature at the laser-SiC substrate interaction zone based on the thermophysical and optical properties of the SI SiC semiconductor.^{2,22} The calculated temperature at the interaction zone between the 355 nm laser and SiC substrate is strongly related to the thermophysical properties of this SiC substrate, laser power, and interaction time. The temperature triggered at the laser-SiC substrate interaction zone can be calculated as follows:²²

$$T(0, \tau_{int}) = T_r + 2 \left(\frac{AP}{ka} \right) \sqrt{\left(\frac{\alpha \tau_{int}}{\pi} \right)}. \quad (2)$$

Here, T_r is the room temperature (300 K) at which the experiments are performed, A is the absorptance of the SiC substrate at $\lambda = 355$ nm, k is the thermal conductivity, and α is the thermal diffusivity of the SiC substrate. P denotes the laser irradiation power, and a is the area of interaction between the laser focal spot and the surface of SiC substrate. Bougdid *et al.*²² used Eq. (2) to select the laser processing parameters for the laser sintering of different nanoparticles, e.g., TiO₂, and used a linear stage to control the motion of the samples during the laser processing.

We previously²² used the simple model based on equation [Eq. (2) in the current paper] to validate the temperature required to sinter TiO₂ nanoparticles on quartz substrate for transparent film applications, and this model was successful in predicting the phase transformation of TiO₂. As reported in Ref. 22, 3.55 W power combined with 2 mm/s substrate speed transforms TiO₂ nanoparticles from the amorphous phase to rutile crystalline phase. Using these process parameters, the temperature was found to be 550–600 °C, which represents the phase transition temperature from amorphous to rutile. During their experiment in Ref.22 with these process parameters, the formation of rutile phase was observed in sinter TiO₂ film in Fig. 8(g) in Ref. 22. Their experimental observation validated the prediction of this simple model/equation [Eq. (2) in the current paper].

The current theoretical calculation of this paper differs significantly in that a galvanometer scanner is used to scan the surface of the SiC substrate. The velocity of the sample during the laser doping process can be determined as follows:

$$v = d\omega. \quad (3)$$

Due to the high optical absorptance of SiC substrate at 355 nm, i.e., the wavelength of the laser used for doping, the absorptivity of our SiC is found to be around ~75%. The laser-material interaction time τ_{int} is given by Eq. (1), where $L_{spot\ size}$ is the laser spot size at the surface of the SiC substrate, and the velocity (scan rate) is given by the Eq. (3). Equation (4) is used to determine the laser spot size at surface of the SiC substrate,²³

$$L_{spot\ size} = \frac{4 f_{lens} \lambda M^2}{\pi d_{beam}} \quad (4)$$

Here, M^2 is a measure of how much the laser output deviate from an idealized Gaussian laser beam. λ is the laser wavelength, f_{lens} is the focal distance of the focusing lens, and d_{beam} is the

29 March 2024 15:15:17

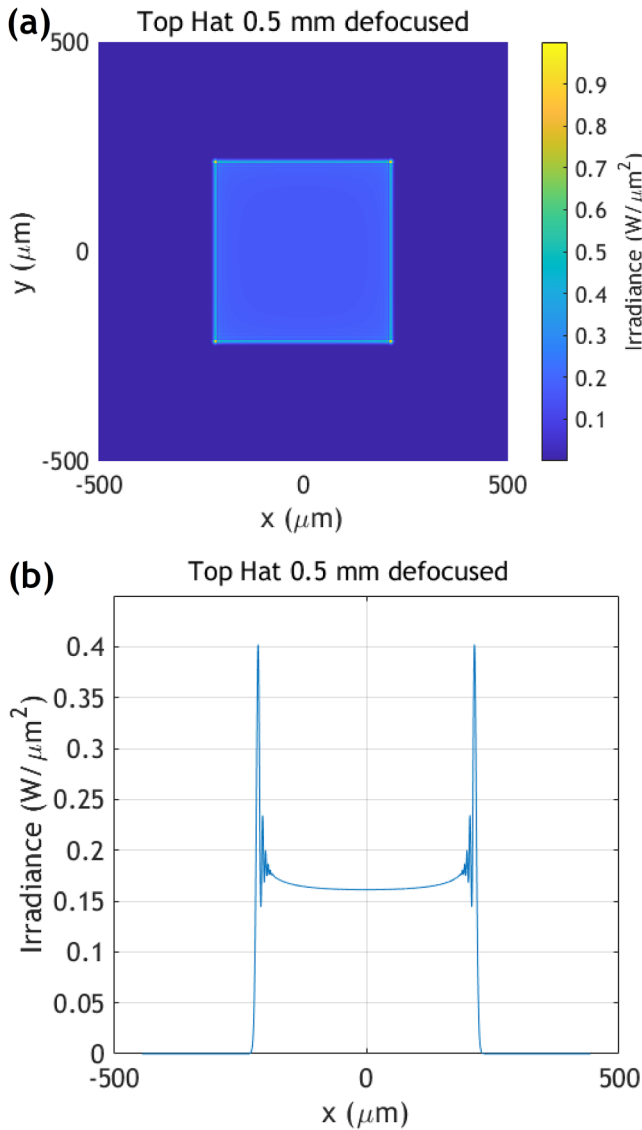


FIG. 10. (a) Peak laser irradiance and (b) peak irradiance x-profile at $z = 0.5$ mm. Laser irradiance is +0.5 mm beyond the focus showing a significant drop in irradiance intensity at sample point SP4 (see Fig. 9).

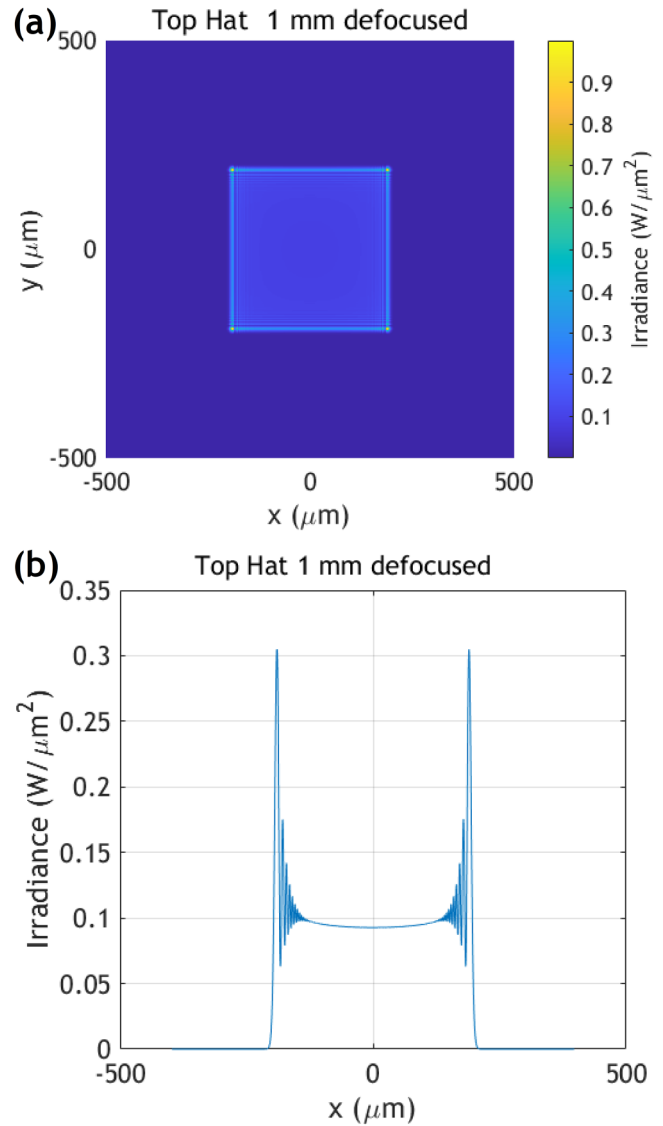


FIG. 11. (a) Peak laser irradiance and (b) peak irradiance x-profile at $z = 1$ mm. Laser irradiance is +1 mm beyond the focus showing a severe drop in irradiance intensity at sample point SP5 (see Fig. 9).

29 March 2024 15:15:17

diameter of the laser beam. From Eq. (2), the two independent parameters, i.e., scan rate and laser power, are simulated and plotted in Fig. 13 to select the proper laser processing parameters for doping of SI HP 4H-SiC substrates. The results in Fig. 13 show that most of the selected processing parameters are below the peritectic temperature of SiC substrate, i.e., 2830 °C according to Ref. 4. Figure 13 shows that with a laser spot size of 0.4 mm diameter, there is sufficient margin to increase the laser spot size and the scan rate. The 355 nm laser source is capable of producing up to 20 W of power; this is plenty of power to reach the required

temperature at a given interaction time to dope the SiC substrates above a certain scan rate while maintaining the temperature below the peritectic temperature of SiC, i.e., 2830 °C.

III. DISCUSSION

The change in the refraction index and absorption index due to the diffusion of boron atoms into the SI HP 4H-SiC substrate will be investigated by FTIR measurements of transmittance and reflectance of the doped SiC samples. SI HP 4H-SiC

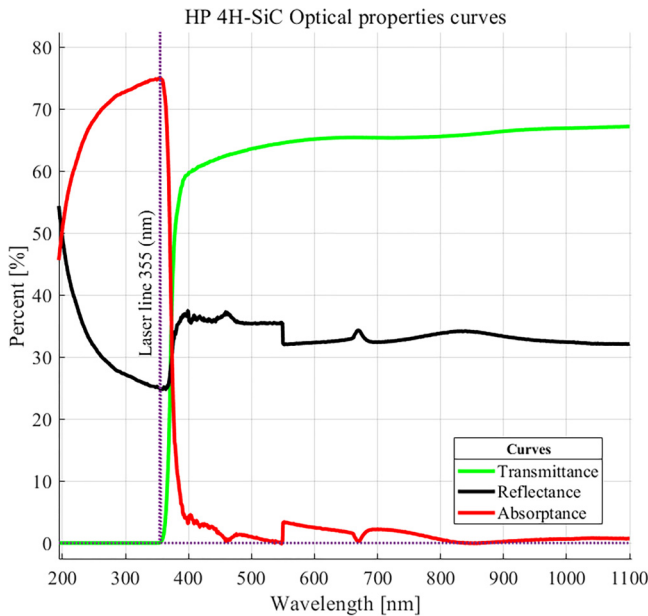


FIG. 12. Measured transmittance, reflectance, and absorptance of the semi-insulating HP SI 4H-SiC substrate (as received) used in this work.

semiconductors substrates can be used as the transport medium to build resonant waveguides for MWIR radiation because of their excellent electrical and optical properties.³ Laser doping of 4H-SiC with dopant, e.g., gallium or boron, atoms can increase the refraction index when the Ga/or B-doped sample is excited by a 4.3 μm wavelength (Lim *et al.*⁴). Accordingly, the optical path lengths of the MWIR radiation can be changed dynamically by traveling through this doped SiC material when excited by the 4.3 μm light source.

SI HP 4H-SiC can be also used as an efficient waveguide material compared to its vanadium-doped counterpart, because SI HP 4H-SiC has fewer scattering sites than SiC doped with vanadium.¹⁷ The Rayleigh scattering introduced by dopants atoms into the SiC substrates increases the optical loss experienced by light as it travels through this semiconductor device. By starting with high-purity semiconductor material, we do not need to use a high concentration of boron dopants in our study to experience the same index change. This additional benefit thereby reduces the propagation loss of transmitted radiation in the doped SiC substrate.

Our laser doping setup was designed to exploit the high absorptance of SI HP 4H-SiC at 355 nm laser radiation. This choice of the heating laser source of 355 nm wavelength reduces the power needed to incorporate the boron atoms into the SI HP SiC by thermal diffusion. Additionally, our current doping setup opens up the processing parameter space for the use of a larger-diameter laser spot and faster scan rates. It is demonstrated through our simulation that a flat-top beam at the focus maintains a peak power density over a larger distribution of the laser beam at the focal spot of the focusing lens, as shown in Fig. 14. Figure 14

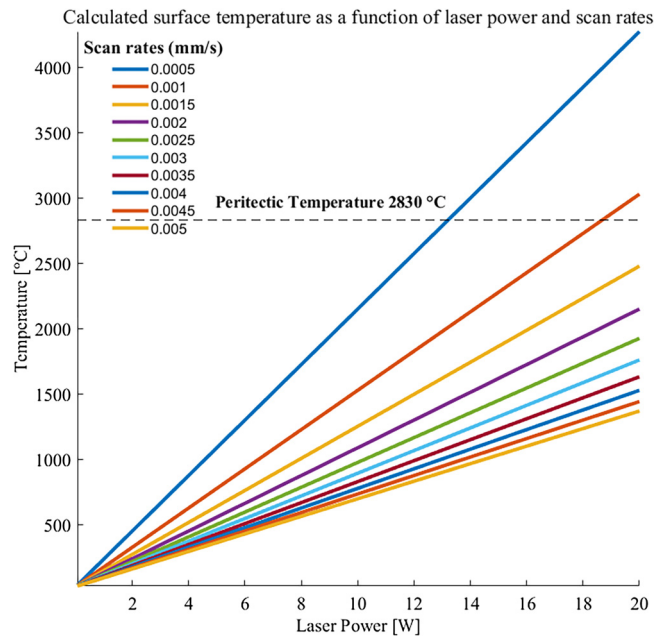


FIG. 13. Calculated temperature for a Gaussian beam at the laser-SiC substrate interaction zone as a function of laser power for different scan rates.

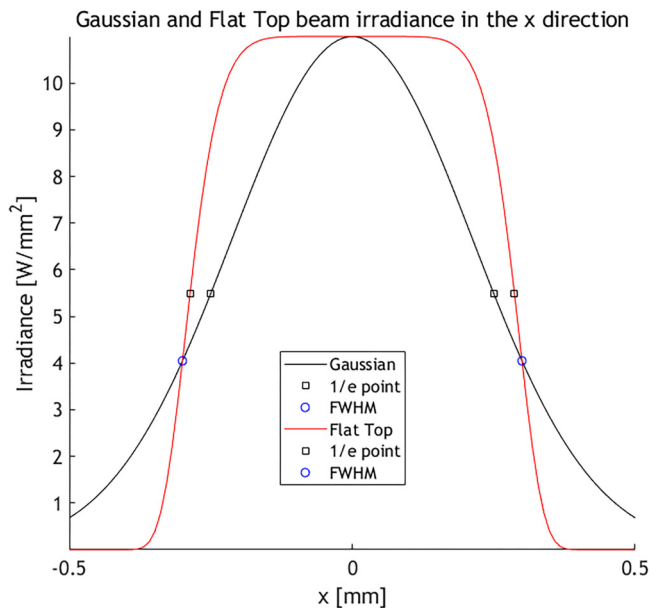


FIG. 14. The visual realization of the irradiance of the Gaussian beam (black) and the flat-top beam (red) irradiance distribution in the x-direction.

29 March 2024 15:15:17

demonstrated the visual realization of power distribution of the Gaussian laser beam versus the flat top irradiance in the lateral direction of the x axis.

The open architecture of our optical setup design would allow one to change the laser spot size fairly easily by swapping out the biconvex lens. An easy operation of our laser optical setup is demonstrated. Additionally, the high absorptance of the 355 nm laser by the 4H-SiC substrates leaves plenty of room to vary the scan rate and stay below the 20 W power limitation from our proposed laser system (Fig. 12). A systematic simulation on predicting the laser processing parameters for doping 4H-SiC substrates with boron is demonstrated in this paper.

IV. SUMMARY

A novel laser doping setup has been developed based on the simulation of the different processing parameters using the optical and electrical characteristics of SI HP 4H-SiC semiconductors. Rayleigh scattering is provided as the reason for using SI HP 4H-SiC as the recording medium semiconductor for creating resonant optical waveguides. Given that this material has a strong optical absorptance at 355 nm, our experiments have been proposed around this UV laser. The optical system response has been simulated given the 4H-SiC characteristic parameters to determine the laser processing parameters, i.e., scan rates, laser spot size, and laser power, which are required to operate and optimize to achieve proper and efficient laser doping of SiC substrates for resonant optical waveguide applications. Our simulation on laser doping of SiC discussed in this paper can be used to minimize the number of experiments used to develop the processing parameters at a lower cost and with high efficiency by changing the experimental parameters in real time and interactively.

ACKNOWLEDGMENTS

The author would like to thank Naval Air Warfare Center Aircraft Division for their support on this project through their Section 219 funding, work force development. Additionally, the authors would like to thank Dr. Justin Lang and Mari Woolridge for the generous use of their time in helping measure the material characteristic data. Finally, the authors would like to thank Dowlat Ram Sugrim for the generous use of his time to create the solid model diagram of our doping platform.

AUTHOR DECLARATIONS

Conflict of Interest

The authors have no conflicts to disclose.

Author Contributions

Chandraika (John) Sugrim: Conceptualization (equal); Data curation (equal); Formal analysis (equal); Investigation (equal); Methodology (equal); Project administration (equal); Resources (equal); Software (equal); Validation (equal); Visualization (equal); Writing – original draft (equal); Writing – review & editing (equal). **Gunjan Kulkarni:** Conceptualization (equal); Data curation (equal); Formal analysis (equal); Investigation (equal); Methodology (equal); Software (equal); Validation (equal); Visualization (equal); Writing –

original draft (equal); Writing – review & editing (equal). **Yahya Bougdid:** Conceptualization (equal); Data curation (equal); Formal analysis (equal); Investigation (equal); Methodology (equal); Software (equal); Validation (equal); Visualization (equal); Writing – original draft (equal); Writing – review & editing (equal). **Kevin Heylman:** Validation (equal); Visualization (equal); Writing – review & editing (equal). **Ranganathan Kumar:** Conceptualization (equal); Data curation (equal); Formal analysis (equal); Investigation (equal); Methodology (equal); Project administration (equal); Resources (equal); Software (equal); Supervision (equal); Validation (equal); Visualization (equal); Writing – original draft (equal); Writing – review & editing (equal). **Aravinda Kar:** Conceptualization (equal); Data curation (equal); Formal analysis (equal); Investigation (equal); Methodology (equal); Project administration (equal); Resources (equal); Software (equal); Supervision (equal); Validation (equal); Visualization (equal); Writing – original draft (equal); Writing – review & editing (equal). **Kalpathy Sundaram:** Conceptualization (equal); Data curation (equal); Formal analysis (equal); Investigation (equal); Methodology (equal); Software (equal); Supervision (equal); Validation (equal); Visualization (equal); Writing – original draft (equal); Writing – review & editing (equal).

REFERENCES

- 1 I. A. Salama, N. R. Quick, and A. Kar, "Laser doping of GaN for advanced optoelectronic applications," in *International Congress on Applications of Lasers & Electro-Optics* (AIP Publishing, LIA Conference Proceedings, 2014), pp. 50–57.
- 2 Z. Han, H. Zhu, Y. Zou, J. Lu, F. Zhu, and Q. Ning, "Band gap regulation and a selective preparation method for single-walled silicon carbide nanotubes," *Results Phys.* **38**, 105658 (2022).
- 3 S. Bet, N. Quick, and A. Kar, "Effect of laser field and thermal stress on diffusion in laser doping of SiC," *Acta Mater.* **55**, 6816–6824 (2007).
- 4 G. Lim and A. Kar, "Effects of laser scans on the diffusion depth and diffusivity of gallium in n-type 4H-SiC during laser doping," *Mater. Sci. Eng. B* **176**, 660–668 (2011).
- 5 G. Lim, "An uncooled mid-wave infrared detector based on optical response of laser-doped silicon carbide," *Electronic Theses and Dissertations*, 4593, 2014, see <https://stars.library.ucf.edu/etd/4593>.
- 6 *Process Technology for Silicon Carbide Devices* (No. 2), edited by C. M. Zetterling (INSPEC, The Institution of Electrical Engineering, London, United Kingdom, 2002).
- 7 E. F. Schubert, *Light-Emitting Diodes* (Cambridge University Press, Cambridge, 2003).
- 8 Q. Zhang, F. Zhang, X. Liu, Z. Yue, X. Chen, and Z. Wan, "Doping of laser-induced graphene and its applications," *Adv. Mater. Technol.* **8**, 2300244 (2023).
- 9 S. Bet, "Laser enhanced doping for silicon carbide white light emitting diodes," *Electronic theses and dissertations*, 3680, 2008, see <https://stars.library.ucf.edu/etd/3680>.
- 10 I. A. Salama, N. R. Quick, and A. Kar, "Laser microprocessing of wide bandgap materials," *Proc. SPIE* **4831**, 549–554 (2003).
- 11 A. V. Suvorov, D. A. Plotkin, V. N. Makarov, and V. N. Svetlov, "Aluminum ion implantation in silicon carbide at high temperature of target," *Mater. Res. Soc. Symp. Proc.* **279**, 415–420 (1993).
- 12 O. Eryu, Y. Okuyama, K. Nakashima, T. Nakata, and M. Watanabe, "Formation of a p-n junction in silicon carbide by aluminium doping at room temperature using a pulsed laser doping method," *Appl. Phys. Lett.* **67**, 2052–2053 (1995).
- 13 A. Ogane, K. Hirata, K. Horiuchi, Y. Nishihara, Y. Takahashi, A. Kitiyanan, and T. Fuyuki, "Laser-doping technique using ultraviolet laser for shallow doping in crystalline silicon solar cell fabrication," *Jpn. J. Appl. Phys.* **48**, 071201 (2009).

- ¹⁴Y. Bougdid and Z. Sekkat, "Voxels optimization in 3D laser nanoprinting," *Sci. Rep.* **10**, 1–8 (2020).
- ¹⁵Y. Bougdid, I. Maouli, A. Rahmouni, K. Mochizuki, I. Bennani, M. Halim, and Z. Sekkat, "Systematic $\lambda/21$ resolution achieved in nanofabrication by two-photon-absorption induced polymerization," *J. Micromech. Microeng.* **29**, 035018 (2019).
- ¹⁶D. Feng, Z. Qin, Q. Ren, S. Sun, Q. Xia, H. Ru, W. Wang, and C. Zhang, "Occurrence forms of major impurity elements in silicon carbide," *Ceram. Int.* **48**, 205–211 (2022).
- ¹⁷R. Olshansky, "Propagation in glass optical waveguides," *Rev. Mod. Phys.* **51**, 341 (1979).
- ¹⁸P. Sutton, "Introduction to Fourier optics," *Quantum Semiclassical Opt. J. Eur. Opt. Soc. B* **8**, 014 (1996).
- ¹⁹J. W. Goodman, *Introduction to Fourier Optics* (McGraw-Hill Inc., 1969), Chap. 4, p. 86.
- ²⁰A. Haghightazadeh and H. Golnabi, "Theoretical modeling of generation of hat-top intensity profile from Gaussian beam by means of a two-stage beam shaper," *Opt. Commun.* **294**, 182–187 (2013).
- ²¹C. Boutopoulos, P. Terzis, I. Zergioti, A. G. Kontos, K. Zekentes, K. Giannakopoulos, and Y. S. Raptis, "Laser annealing of Al implanted silicon carbide structural and optical characterization," *Appl. Surf. Sci.* **253**, 7912–7916 (2007).
- ²²Y. Bougdid, F. Chenard, J. Sugrim, R. Kumar, and A. Kar, "CO₂ laser-assisted sintering of TiO₂ nanoparticles for transparent films," *J. Laser Appl.* **35**, 012012 (2023).
- ²³B. E. Saleh and M. C. Teich, *Fundamentals of Photonics*, 1st ed. (Wiley, New York, 1991), p. 94.